Cooling rates and energy partition in inhomogeneous fluidized granular mixtures

J. Javier Brey and M. J. Ruiz-Montero
Física Teórica, Universidad de Sevilla, Apartado de Correos 1065, ES-41080, Sevilla, Spain
(Received 23 May 2011; published 7 September 2011)

The local cooling rates of the components of a vibrated binary granular mixture in a steady state are investigated. The accuracy of the expression obtained by assuming a local homogeneous cooling state distribution of the gas is analyzed by comparing it with molecular dynamics simulation results. A good agreement is observed. Also, the profiles of the partial temperatures are compared with the theoretical prediction following from the application of the Chapman-Enskog method to solve the kinetic Enskog equations of the mixture. In this case, the agreement is satisfactory if the boundary layers near the walls are excluded. The implications of the results are discussed.

DOI: 10.1103/PhysRevE.84.031302 PACS number(s): 45.70.Mg, 51.10.+y, 05.20.Dd

I. INTRODUCTION

As a consequence of the inelasticity of collisions, granular fluids exhibit a series of behaviors that are in sharp contrast with those of molecular fluids. One of them is the violation of the energy equipartition theorem in a granular mixture of mechanically different species. The granular temperatures of the components of the mixture, defined from the average kinetic energies, are different. Although this possibility was already pointed out many years ago [1], it has not been until recently that a systematic study of the effect has been started. For the homogeneous state of a freely cooling binary mixture of inelastic hard spheres or disks, an explicit expression for the ratio of the temperatures of the two components has been obtained from an approximated solution of the kinetic Enskog equations [2]. The accuracy of this prediction for weak dissipation and low density has been confirmed by molecular dynamics (MD) simulations [3].

The above homogeneous cooling state (HCS) is not accessible experimentally since it is of too short a duration to be observed. In order to maintain a granular system fluidized, an external energy supply is required. This is often carried out in experiments by means of vibrating walls or external fields, which generate macroscopic gradients in the system because of the inelasticity. At a theoretical level, *homogeneously driven* granular fluids have also been considered. In these models, external stochastic forces giving energy to the particles are added, thus allowing a system of inelastic particles otherwise isolated to reach a steady state. The lack of energy equipartition in the steady state of homogeneously driven granular mixtures has been also analyzed [4] by extending the methods of [2]. Nevertheless, the relationship between this kind of driving and actual experiments is uncertain. The nonequipartition has also been identified in simple shear flows in which the density and the temperature are uniform [5] and observed in MD simulations of vibrated granular gases [6,7]. In the latter cases, the parameter characterizing the departure from energy equipartition, for instance, the ratio of the partial temperatures of the components, exhibits a local, position dependent behavior.

In addition, experimental evidence of the coexistence of different temperatures in strongly vibrated granular mixtures has been reported in both two- [8] and three-dimensional [9] systems and the dependence of the temperature ratio on the several parameters characterizing the system has been investigated.

Theoretical predictions for the local value of the temperature ratio in a binary mixture of granular gases in inhomogeneous states follow as a by-product in the derivation of hydrodynamic equations in the context of kinetic theory [10–12]. This feature is often forgotten, although it is closely related with important conceptual issues dealing with the existence itself of a hydrodynamic description and with the Chapman-Enskog method to derive the corresponding macroscopic equations. One of the aims of this paper is to emphasize the generality of the theoretical prediction for the partial temperatures of the components of a mixture in states that are described by the hydrodynamic equations to Navier-Stokes order. Quite peculiarly, the expression for the temperature ratio turns out to be independent of the gradients of the hydrodynamic fields, only depending on the local values of the densities of the two components.

The qualitative and quantitative validity of the theory will be investigated by comparing it with MD simulation results for a vibrated granular gas of inelastic hard disks in a highly inhomogeneous state. In the analysis, a crucial role is played by the local cooling rates of the fluid and of each of the components. In most of the hydrodynamic theories of monocomponent and multicomponent granular gases, the exact local cooling rates are approximated, without any well founded justification, by its zeroth order in the gradients of the hydrodynamic fields, which, in addition, is computed by using a Gaussian approximation for the local velocity distributions [13]. The issue of the validity of this assumption is also addressed in the MD analysis being reported below. It will be shown that the actual local energy dissipation in the system is very well described by assuming local Gaussian distributions for the components, at least for not too strong inelasticity. Neither zeroth order in the gradients' deviations from a Gaussian nor corrections associated with the gradients of the hydrodynamic fields seem to be quantitatively relevant to describe the cooling rate of the system. This provides justification for the expression of the cooling rate generally used in the hydrodynamic equations for systems of smooth inelastic hard spheres and disks.

The remainder of the paper is organized as follows. In the next section, the theoretical results for the cooling rates and the partial temperatures are reviewed. They follow from the

application of the Chapman-Enskog method to the Enskog equations of the system. It is emphasized as to which aspects have a justification on physics grounds, and as to which ones are a consequence of some mathematical approximation or choice. This is important to understand the basis of the equation determining the ratio of the partial local temperatures of the components as a function of the concentration profiles. In Sec. III, MD simulation results are presented for a vibrated system of inelastic hard disks in a steady state. The partial cooling rates and temperatures are measured, and the results compared with the theoretical predictions. The final section of the paper contains a short summary of the results, and also the comparison of the theory with some previous simulation results and experiments.

II. BOLTZMANN-ENSKOG EQUATION AND CHAPMAN-ENSKOG SOLUTION

We consider a mixture of smooth inelastic hard spheres ($d = 3$) or disks ($d = 2$) of masses m_1 and m_2 and diameters σ_1 and σ_2. The inelasticity of collisions is modeled by constant coefficients of normal restitution. There are three of them: α_{11}, α_{22}, and $\alpha_{12} = \alpha_{21}$, where α_{ij} refers to collisions between a particle of species i and a particle of species j. They are defined in the interval $0 < \alpha_{ij} \leqslant 1$. We also introduce $\sigma_{ij} = (\sigma_i + \sigma_j)/2$. The particles are submitted to an external field, so the force acting on a particle of species i is $\boldsymbol{F}_i$.

The Enskog equations for the one-particle distribution functions $f_i(\boldsymbol{r},\boldsymbol{v},t)$, $i = 1,2$, have the form [14]

$$\left(\partial_t + \boldsymbol{v}\cdot\nabla + \frac{\boldsymbol{F}_i}{m_i}\cdot\frac{\partial}{\partial \boldsymbol{v}}\right) f_i(\boldsymbol{r},\boldsymbol{v},t) = \sum_{j=1,2} J_{ij}[\boldsymbol{r},\boldsymbol{v}|f_i,f_j], \tag{1}$$

where J_{ij} is the inelastic Enskog collision operator for the scattering of a particle of species i and a particle of species j. Below, the application of the Chapman-Enskog algorithm to Eq. (1), as carried out in Ref. [10], will be shortly reviewed. Emphasis will be put on those conceptual issues and hypothesis motivating the study presented here.

The important first step in any derivation of macroscopic continuum equations is the choice of the fields. And it must be stressed that the Chapman-Enskog procedure does not make any explicit limitation on the fields to be used. The only required condition is the existence of a uniform reference state than can be expressed in terms of the chosen fields. In particular, for granular mixtures, two sets of fields have been considered for hydrodynamic descriptions. One is formed by the number densities of the species, the flow velocity associated with the total momentum, and the granular temperature defined from the total energy density [10]. The second set consists of the number densities, species flow velocities defined from the species momenta, and species granular temperatures defined from the local species energies [1,15]. The point of view adopted here is that the expanded set does not have a larger predictive value on the relevant large space and time scales. A discussion of this issue is carried out in Ref. [16]. Here, let us mention that the accuracy of using the reduced set has been confirmed by molecular dynamics simulations both in the homogeneous case [3,17] and also in inhomogeneous vibrated mixtures [18].

The macroscopic field's number density of species i, $n_i(\boldsymbol{r},t)$, flow velocity $\boldsymbol{u}(\boldsymbol{r},t)$, and granular temperature $T(\boldsymbol{r},t)$, are defined in the usual way:

$$n_i = \int d\boldsymbol{v}\, f_i(\boldsymbol{r},\boldsymbol{v},t), \quad \rho\boldsymbol{u} = \sum_i \int d\boldsymbol{v}\, m_i \boldsymbol{v} f_i(\boldsymbol{r},\boldsymbol{v},t),$$
$$nT = \sum_i \int d\boldsymbol{v}\, \frac{m_i V^2(\boldsymbol{r},t)}{d} f_i(\boldsymbol{r},\boldsymbol{v},t). \tag{2}$$

Here, $\rho = m_1 n_1 + m_2 n_2$ is the total mass density, $n = n_1 + n_2$ is the total number density, and $\boldsymbol{V} = \boldsymbol{v} - \boldsymbol{u}$ is the peculiar velocity. Balance equations for the above fields are derived from the set of Enskog equations (1):

$$\partial_t n_i + \nabla\cdot(n\boldsymbol{u}) + m_i^{-1}\nabla\cdot\boldsymbol{j}_i = 0, \tag{3}$$

$$\partial_t \boldsymbol{u} + \boldsymbol{u}\cdot\nabla\boldsymbol{u} + \rho^{-1}\nabla\cdot\mathsf{P} - \rho^{-1}\sum_i n_i \boldsymbol{F}_i = 0, \tag{4}$$

$$\partial_t T + \boldsymbol{u}\cdot\nabla T - n^{-1}\sum_i m_i^{-1}[T\nabla + 2(d)^{-1}\boldsymbol{F}_i]\cdot\boldsymbol{j}_i$$
$$+ 2(nd)^{-1}(\nabla\cdot\boldsymbol{q} + \mathsf{P}:\nabla\boldsymbol{u}) + T\zeta = 0, \tag{5}$$

where $\boldsymbol{j}_i$ is the mass flow for species i relative to the local flow, P is the pressure tensor, and $\boldsymbol{q}$ is the heat flux. The definitions of these fluxes will not be needed in the following. In addition, Eq. (5) contains the cooling rate ζ due to the inelasticity of collisions,

$$\zeta(\boldsymbol{r},t) = -(nTd)^{-1}\sum_{i,j}\int d\boldsymbol{v}\, m_i v^2 J_{ij}[\boldsymbol{r},\boldsymbol{v}|f_i,f_j]. \tag{6}$$

The balance equations become a closed set of hydrodynamic equations for the macroscopic fields once $\boldsymbol{j}_i$, P, $\boldsymbol{q}$, and ζ are expressed as functionals of these fields. This requires us to find a solution to the Enskog equations such that all the space and time dependence occurs through the hydrodynamic fields [10]

$$f_i(\boldsymbol{r},\boldsymbol{v},t) = f_i\left[\boldsymbol{v}|n_1(\boldsymbol{r},t),n_2(\boldsymbol{r},t),\boldsymbol{u}(\boldsymbol{r},t),T(\boldsymbol{r},t)\right]. \tag{7}$$

In the Chapman-Enskog procedure, this "normal solution" is generated by representing it as a series expansion in a formal nonuniformity parameter ϵ, $f_i = f_i^{(0)} + \epsilon f_i^{(1)} + \epsilon^2 f_i^{(2)} + \cdots$, where each factor of ϵ indicates an implicit gradient of a macroscopic field. Use of this expansion in the definition of the fluxes and the cooling rates gives a corresponding expansion for them. In this way, the time derivatives of the fields can also be expanded in powers of ϵ. Then, to zeroth order in ϵ, it is easily obtained [12]:

$$-\zeta^{(0)} T\frac{\partial}{\partial T} f_i^{(0)} = \sum_j J_{ij}^{(0)}\left[\boldsymbol{v}\middle|f_i^{(0)},f_j^{(0)}\right], \tag{8}$$

$$J_{ij}^{(0)}\left[\boldsymbol{v}\middle|f_i^{(0)},f_j^{(0)}\right] = g_{ij}(\sigma_{ij}) J_{B,ij}\left[\boldsymbol{v}\middle|f_i^{(0)},f_j^{(0)}\right], \tag{9}$$

where $J_{B,ij}$ is the inelastic Boltzmann collision operator for particles of species i and j, and $g_{ij}(\sigma_{ij})$ is the equilibrium pair distribution function for species i and j at contact and evaluated at the local densities $n_i(\boldsymbol{r},t)$. The lowest order

cooling rate $\zeta^{(0)}$ is obtained by particularizing Eq. (6) to zeroth order in the gradients:

$$\zeta^{(0)}(\boldsymbol{r},t) = -(nTd)^{-1}\sum_{i,j}\int d\boldsymbol{v}\, m_i v^2 J_{ij}^{(0)}\left[\boldsymbol{v}\middle| f_i^{(0)}, f_j^{(0)}\right]. \quad (10)$$

The solutions to Eq. (8) are chosen such that they have the same moments as in Eq. (2) for all $\boldsymbol{r}$,t:

$$\int d\boldsymbol{v}\, f_i^{(0)} = n_i, \quad (11)$$

$$\sum_i \int d\boldsymbol{v}\, m_i \boldsymbol{v} f_i^{(0)} = \rho \boldsymbol{u}, \quad (12)$$

$$\sum_i \int d\boldsymbol{v}\, m_i V^2 f_i^{(0)} = dn\, T. \quad (13)$$

The above conditions are the generalization of those verified in the elastic case, guaranteeing the existence and uniqueness of solutions to the equations generated to all orders in ϵ by the Chapman-Enskog method [19].

The functions $f_i^{(0)}$ are easily constructed from the distribution functions defining the HCS, through the replacements of the constant uniform fields number densities and temperature by $n_i(\boldsymbol{r},t)$ and $T(\boldsymbol{r},t)$, and substituting $\boldsymbol{v}$ by $\boldsymbol{V}(\boldsymbol{r},t)$. This gives the local HCS distributions, which play a role similar to the local equilibrium distributions in molecular gases. Dimensional analysis requires [2]

$$f_i^{(0)}(\boldsymbol{r},\boldsymbol{v},t) = n_i v_0^{-d}(t)\chi_i\left[\boldsymbol{V}/v_0(t), n_1\sigma_1^d, n_2\sigma_2^d\right], \quad (14)$$

where χ_i is an isotropic function of $\boldsymbol{V}$ and $v_0(t) = [2T(m_1+m_2)/m_1m_2]^{1/2}$ is a local thermal velocity of the mixture. Zeroth-order partial temperatures of the species $T_i^{(0)}(\boldsymbol{r},t)$ can be defined through

$$\int d\boldsymbol{v}\, V^2 f_i^{(0)}(\boldsymbol{r},\boldsymbol{v},t) = m_i^{-1} dn_i T_i^{(0)}. \quad (15)$$

From Eqs. (13) and (15), it follows that $n_1T_1^{(0)} + n_2T_2^{(0)} = nT$. Moreover, Eq. (14) and the definition of the partial temperatures $T_i^{(0)}$ imply that $\gamma^{(0)} \equiv T_1^{(0)}(\boldsymbol{r},t)/T_2^{(0)}(\boldsymbol{r},t)$ is a function of only the local densities n_1 and n_2. This function can be determined as follows. Use of Eq. (14) into Eq. (10) shows that the latter is equivalent to [2]

$$\frac{\zeta_0}{2}\frac{\partial}{\partial \boldsymbol{V}}\cdot\left[\boldsymbol{V} f_i^{(0)}(\boldsymbol{r},\boldsymbol{v},t)\right] = \sum_j J_{ij}^{(0)}\left[\boldsymbol{v}\middle| f_i^{(0)}, f_j^{(0)}\right]. \quad (16)$$

Then, multiplication by m_iV^2 and integration over $\boldsymbol{V}$ yields

$$\zeta^{(0)}(\boldsymbol{r},t) = \zeta_i^{(0)}(\boldsymbol{r},t) \quad (17)$$

with

$$\zeta_i^{(0)}(\boldsymbol{r},t) = -\left(n_iT_i^{(0)}d\right)^{-1}\sum_j\int d\boldsymbol{v}\, m_i V^2 J_{ij}^{(0)}\left[\boldsymbol{v}\middle| f_i^{(0)}, f_j^{(0)}\right]. \quad (18)$$

If this expression is particularized for the HCS, $\zeta_i^{(0)}$ becomes the partial cooling rate associated with the temperature $T_i^{(0)}(t)$.

The evaluation of $\zeta_i^{(0)}$ requires us to solve consistently the coupled set of equations (8). This can be done in a systematic way by expanding $f_i^{(0)}$ in terms of an ensemble of orthogonal polynomials [2]. Here, we will use a leading order approximation, which is expected to give quite accurate results, at least for not very strong inelasticity. The lowest order distribution functions appearing in Eq. (17) are approximated by Gaussians

$$f_i^{(0)}(\boldsymbol{r},\boldsymbol{v},t) = n_i(\boldsymbol{r},t)\left[\frac{2\pi T_i^{(0)}(\boldsymbol{r},t)}{m_i}\right]^{-d/2} e^{-mV^2/2T_i^{(0)}(\boldsymbol{r},t)}. \quad (19)$$

Using this expression, it is straightforward to calculate the right-hand side of Eq. (17). The technical details needed to evaluate the integrals have already been given several times [2,4,20] and will be not reproduced here. The result is

$$\zeta_1^{(0)} = \frac{2\pi^{(d-1)/2}}{\Gamma(d/2)d}\left\{\left[\frac{T_1^{(0)}}{m_1}\right]^{1/2}(1-\alpha_{11}^2)\sigma_{11}^{d-1}n_1g_{11} + 4\sqrt{2}\left[\frac{T_2^{(0)}}{m_2}\right]^{1/2}\sigma_{ij}^{d-1}n_2g_{12}h_{12} \times\left[1-\frac{h_{12}(1+\phi)}{\phi}\right](1+\phi)^{1/2}\right\}, \quad (20)$$

where

$$h_{ij} \equiv \frac{m_j(1+\alpha_{ij})}{2} \quad (21)$$

and

$$\phi \equiv \frac{m_2T_1^{(0)}}{m_1T_2^{(0)}}. \quad (22)$$

Of course, the expression for $\zeta_2^{(0)}$ follows from Eq. (20) by interchanging 1 and 2 and, consistently, changing ϕ into ϕ^{-1}. Thus, the requirement $\zeta_1^{(0)} = \zeta_2^{(0)}$ leads to

$$\phi^{1/2}(1-\alpha_{11}^2)\left(\frac{\sigma_1}{\sigma_{12}}\right)^{d/2}\frac{n_1}{n_2}g_{11}(\sigma_1) + 4\sqrt{2}h_{12}\left[1-\frac{h_{12}(1+\phi)}{\phi}\right](1+\phi)^{1/2}g_{12}(\sigma_{12}) - \left(1-\alpha_{22}^2\right)\left(\frac{\sigma_2}{\sigma_{12}}\right)^{d-1}g_{22}(\sigma_2) - 4\sqrt{2}\frac{n_1}{n_2}h_{21} \times[1-h_{21}(1+\phi)](1+\phi)^{1/2}g_{12}(\sigma_{12}) = 0. \quad (23)$$

This equation is formally the same as for the homogeneous cooling state [2], but with the global fields substituted by the local ones as first noticed in Ref. [10]. The solution of this equation provides $\gamma^{(0)} \equiv T_1^{(0)}(\boldsymbol{r},t)/T_2^{(0)}(\boldsymbol{r},t)$ as a function of $n_1(\boldsymbol{r},t)/n_2(\boldsymbol{r},t)$ and the values of the equilibrium pair correlations at contact, consistently with the discussion below Eq. (12). In principle, this result is not very useful for granular mixtures that are not in the HCS since the temperature parameters $T_i^{(0)}$ do not provide the actual energy densities of the components of the mixture, but their lowest order approximation in some gradient expansion. The case of a mixture in the tracer limit $n_1/n_2 \to 0$ has been previously considered in [21,22]. There, an equation corresponding to the appropriate limit of Eq. (23) was derived. In addition, the

property $T_i^{(0)} = T_i$ is verified, where T_i is the actual partial granular temperature of species i defined by

$$\int d\boldsymbol{v}\, V^2 f_i(\boldsymbol{r},\boldsymbol{v},t) = m_i^{-1} dn_i T_i. \tag{24}$$

Therefore, Eq. (23) determines the local energy partition in the system. Moreover, these predictions were shown to be in quite good agreement with MD results for a vibrated low-density granular gas [$g_{ij}(\sigma_{ij}) = 1$] in the presence of gravity.

What about the general case wherein the composition of the mixture does not correspond to the tracer limit? Note that the solubility conditions given by Eqs. (11)–(13) do not imply any relationship between the lowest order parameters $T_i^{(0)}$ and the actual partial temperatures T_i, other than $n_1 T_1^{(0)} + n_2 T_2^{(0)} = nT$. Nevertheless, additional information follows from the derivation of the hydrodynamic equations with explicit expressions for the transport coefficients. The practical implementation of the Chapman-Enskog procedure requires us to expand the distribution functions in some set of orthogonal polynomials in order to get explicit expressions for the hydrodynamic fluxes and the cooling rate. Usually, the Sonine polynomial expansion is employed [23,24]. This is what is also done in Refs. [10–12] for granular mixtures of inelastic hard spheres or disks. And, it happens that the corrections to the lowest order distribution functions $f_i^{(0)}$ do not contribute to the second velocity moment, i.e., $T_i^{(0)} = T_i$, as a consequence of the orthogonality property of the Sonine polynomials. The conclusion is that Eq. (23) also determines the ratio $\gamma \equiv T_1/T_2$ since it agrees with $\gamma^{(0)}$.

Equation (23) may appear as surprisingly simple, especially taking into account its generality. No particular state of the mixture has been considered. This is a consequence of the assumption that there is a hydrodynamic description in terms of only n_1, n_2, $\boldsymbol{u}$, and T, as well as of the use of the Chapman-Enskog procedure, including the expansion in orthogonal polynomials, to generate it. Although the partial temperatures T_i of the two components are different, they are not needed to specify the macroscopic state of the mixture. Moreover, the theory provides a relationship to determine them as a function of the assumed hydrodynamic fields. This relation has a local character and does not involve the gradients of those fields nor the external force. The local relation between the partial temperatures is the same as in the HCS. This does not imply any kind of *local HCS approximation*, in the same way as equipartition in molecular systems does not imply local equilibrium. The above results would not apply if the characterization of the macroscopic state of the mixture would require us to specify the partial temperatures of the components and, therefore, they should be included into the set of independent hydrodynamic fields. Of course, in this case, one more hydrodynamic equation, with the corresponding new transport coefficients, is required. This is the kind of approximation followed in [1].

For a practical application of Eq. (23) beyond the very dilute limit, explicit expressions for $g_{ij}(\sigma_{ij})$ are needed. For $d = 3$,

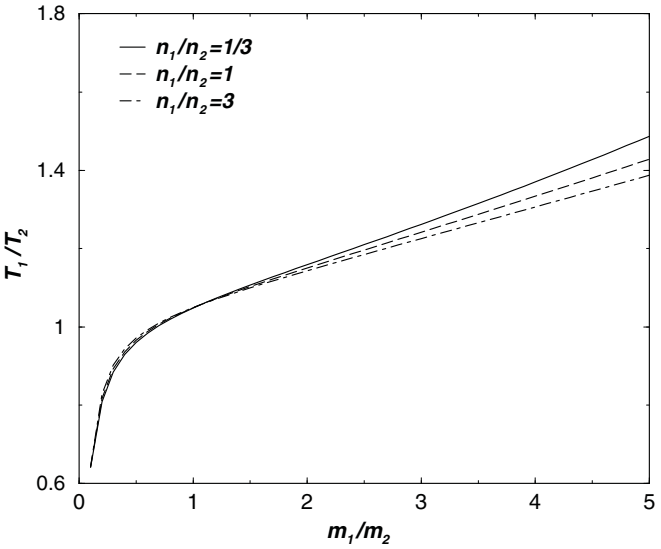

FIG. 1. Temperature ratio $\gamma = T_1/T_2$ given by Eq. (23) as a function of the mass ratio m_1/m_2 for $d = 2$, $\alpha_{11} = 0.9$, $\alpha_{22} = 0.8$, and $\alpha_{12} = 0.85$. The diameters of the two kinds of particles are the same and the area fraction is $\nu = 0.1$

the extended Carnahan-Stirling form [25]

$$g_{ij}(\sigma_{ij}) = \frac{1}{1-\nu} + \frac{3\xi}{2(1-\nu)^2}\frac{\sigma_i\sigma_j}{\sigma_{ij}} + \frac{\xi^2}{2(1-\nu)^3}\left(\frac{\sigma_i\sigma_j}{\sigma_{ij}}\right)^2 \tag{25}$$

can be used. Here, $\nu \equiv (\pi/6)\sum n_i\sigma^3$ is the mixture volume fraction and $\xi \equiv (\pi/6)\sum_i n_i\sigma_i^2$. The corresponding expression for $d = 2$ is [26]

$$g_{ij}(\sigma_{ij}) = \frac{1}{1-\nu} + \frac{9\xi}{16(1-\nu)^2}\frac{\sigma_i\sigma_j}{\sigma_{ij}}, \tag{26}$$

where now $\nu \equiv (\pi/4)\sum_i n_i\sigma_i^2$, the mixture area fraction, and $\xi \equiv (\pi/4)\sum_i n_i\sigma_i$.

The solution of Eq. (23) for $\gamma^{(0)} = \gamma = T_1/T_2$ depends very weakly on the values of n_1/n_2 for given values of the other parameters. The dependence on the mass ratio and on the diameter ratio is much stronger. To illustrate this, in Fig. 1, the theoretical prediction for γ is plotted as a function of m_1/m_2 for three values of n_1/n_2, namely, 1/3, 1, and 3. The other relevant parameters are $d = 2$, $\alpha_{11} = 0.9$, $\alpha_{12} = 0.85$, $\alpha_{22} = 0.8$, $\sigma_1 = \sigma_2$, and $\nu = 0.1$. Similar results are obtained for other values of these parameters. This property plays an important role in the analysis of both MD and experimental results.

III. MD RESULTS FOR A VIBRATED GRANULAR MIXTURE

We have performed event-driven molecular dynamics simulations of a binary mixture of inelastic hard disks ($d = 2$) in the presence of a gravitational field, i.e., $\boldsymbol{F}_i = -m_i g_0 \widehat{\boldsymbol{e}}_z$, where g_0 is a constant and $\widehat{\boldsymbol{e}}_z$ the unit vector in the positive direction of the Z axis. The system is confined in a box of width W and it is open on the top. Periodic boundary conditions are used in the horizontal direction. Energy is supplied through the wall at the bottom, which is vibrating with a sawtooth velocity

profile, so that particles colliding with it always find the wall moving upward with the same velocity v_W. Also, the limit of small amplitude of the oscillations as compared with the mean free path of the gas in the vicinity of the vibrating wall is considered. This allows us to treat the position of the wall as fixed at $z = 0$ [27,28]. The particle-wall collisions are elastic.

The total number of particles was the same in all the simulations, $N = 420$, being evenly distributed between the two species, i.e., $N_1 = N_2 = N/2$. Since the interest here is on some relationships between hydrodynamic quantities that are expected to apply in the bulk of the system, the only relevant role to be played by the vibrating wall is to maintain the system fluidized. In addition, the value of the velocity of the wall v_W has been chosen such that the density of the system is relatively low. More precisely, we have controlled that the maximum local density in the system is always below $n \sim 0.15\sigma_{12}^{-2}$. Although this value is well above the dilute (Boltzmann) limit, so some finite density effects show up in the system, the Enskog description considered in the preceding section is expected to be able to capture them. Since, in the range of density considered, the disparity in the sizes of the particles must play a minor role in the qualitative features of the system, the diameters of the two species particles have been taken the same in all the simulations, i.e., $\sigma_1 = \sigma_2 = \sigma$.

Under the above conditions, it is known that a one-component granular system reaches a stationary state with only gradients in the direction of the external field [28]. Nevertheless, this state becomes unstable and transversal inhomogeneities are developed in the system when the width W is larger than a critical value [29]. Although we are not aware of any similar analysis for the case of a granular mixture, in all the simulations to be reported in the following, the system was observed to stay homogeneous in the transversal direction. The width of the container was $W = 70\sigma$.

The coefficient of normal restitution for collisions between particles of different species has been fixed according with the rule $\alpha_{12} = (\alpha_{11} + \alpha_{22})/2$. The range of values of these coefficients considered has been restricted to $\alpha_{ii} \geqslant 0.9$. The reason for this limitation is that for larger inelasticities, gradients in the system become very large because of the coupling between inelasticity and gradients of the fields, which is peculiar of many steady states of granular flows. Consequently, the hydrodynamic description provided by the Navier-Stokes order does not hold for such values of the coefficient of normal restitution.

In the simulations, the system has been left to evolve from an arbitrary initial condition until it reaches a stationary state. Then, the quantities of interest have been measured and averaged over different time instants and trajectories. The duration of the sampling interval was 4000 collisions per particle, and 20 trajectories were considered in each case. To measure the dependence on height of the properties, the system was divided in layers Δz. In particular, the local cooling rate of species i, $\zeta_i(z)$, has been computed by measuring the variation in kinetic energy $\Delta E_{k,i}(z,\tau)$ of particles of that species in the layer located at z due to collisions during a time interval τ. Then, the local cooling rate is given by

$$\zeta_i(z) = \frac{1}{\langle E_{k,i}\rangle_z}\frac{\Delta E_{k,i}(z,\tau)}{\tau}, \tag{27}$$

where $\langle E_{k,i}\rangle_z$ is the average kinetic energy of particles of species i at height z. In the steady state, the cooling rate is independent of time.

A. One-component system

Before reporting the simulation results for the mixture, some data for a one-component system ($m_1 = m_2$ and $\alpha_{11} = \alpha_{22}$) will be presented. The motivation for it is to investigate the validity of the expression for the cooling rate derived to lowest order in the gradients, i.e., in a *local* HCS, to describe the cooling in a system with gradients of the hydrodynamic fields. As mentioned in the Introduction, this approximation is implicit in all the hydrodynamic equations for granular fluids being used currently. Quite surprisingly, direct measures of the cooling rate from the energy loss in collisions occurring in inhomogeneous systems by means of MD simulations are scarce [30].

In Fig. 2, the profiles of the hydrodynamic fields and the cooling rate for a system with $\alpha = 0.9$ are displayed. This value of the coefficient of normal restitution is close to the limit for which the Navier-Stokes equations of the granular gas provide an accurate description. The upper plot shows the density and temperature profiles, the latter one divided by some arbitrary temperature T_A to plot it on the same scale as the density. The profiles exhibit the well known features of this state [28]: the density has a maximum at a given height, and the temperature first decays, but then it has a minimum and

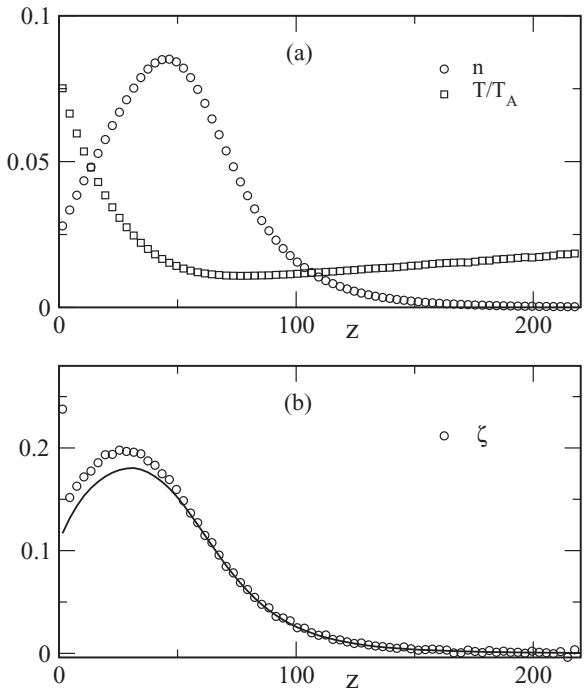

FIG. 2. Profiles for a one-component system with $\alpha = 0.9$. Length is measured in units of the diameter of the particles σ. Figure (a) shows the dimensionless density $n\sigma^2$ (circles) and temperature T/T_A (squares) profiles from the simulation, while figure (b) shows the dimensionless cooling rate $\zeta\,(\sigma/g_0)^{1/2}$. In the latter, the symbols are from the simulation and the solid line is the Gaussian HCS value using the measured local fields.

increases with height from there on. The slope of this increase is larger the more inelastic the system, and it is due to the coupling between heat flux and density gradient that exists in granular fluids [31]. In the bottom plot, the local cooling rate ζ is displayed. It is seen that it is highly inhomogeneous in the system. In the figure, the symbols are data from the simulations and the solid line is the HCS expression, substituting the density and temperature by their local values obtained in the simulations and shown in the upper plot. It corresponds to the Gaussian approximation for the velocity distribution of the gas, as employed to derive Eq. (20). Although expressions for the cooling rate of the HCS have been obtained by including also the first Sonine correction of the distribution function [32,33], it is seen that already the Gaussian approximation provides an accurate expression for the range of inelasticity being considered here. This is especially true in the bulk of the system, outside a boundary layer close to the vibrating wall, in which a deviation of the local cooling rate from its HCS value is observed. This boundary layer is larger the more inelastic the collisions (smaller α) and the simulation results suggest it extends roughly up to the location of the density maximum. Also, for large enough heights, a nonhydrodynamic boundary layer must be observed. Similar results have been obtained for systems with $0.9 \leqslant \alpha < 1$. The agreement between theory and simulation results for the cooling rate improves as the value of the coefficient of normal restitution approaches unity.

B. Binary mixture

Next, results for binary mixtures will be discussed. Consider first a system with $\alpha_{11} = 0.92$ and $\alpha_{22} = 0.98$ ($\alpha_{12} = 0.95$). These values are well outside the quasielastic limit, but still in the range in which the hydrodynamic description to Navier-Stokes order is expected to hold. Keeping these parameters fixed, the effect of changing the mass ratio m_2/m_1 will be studied. In Fig. 3, the profiles for a system with $m_2 = m_1$ are presented. The upper left plot shows the density profile for each of the components as obtained from the simulations. They are seen to be almost identical. The partial temperature profiles are given in the upper right part of the figure. Both simulation results (symbols) and theoretical predictions (solid and dashed lines) are shown. The latter have been obtained by using the expressions

$$T_1 = \frac{nT}{n_2 + \gamma n_1}, \quad T_2 = \frac{\gamma nT}{n_2 + \gamma n_1}, \tag{28}$$

where n_1 and n_2 and T are obtained from the simulations, and γ has been determined by solving Eq. (23), as discussed in the previous section. It is observed that, although both partial temperatures are similar, T_2 is slightly larger than T_1 everywhere in the system. For large z, both partial temperatures increase with the height, a clear indication of the coupling between heat flux and density gradient, already mentioned above. The bottom left plots are the local cooling rates of each of the two components. The symbols are the values obtained directly from the simulation data for the energy dissipated in collisions and using Eq. (27), while the lines correspond to Eq. (20), substituting the densities and the temperatures by the values measured in the simulations. Two relevant features follow from the observation of this figure: The values of the cooling rates are very well fitted by the local HCS value, except in the boundary layer close to the vibrating wall, and the cooling rates of both components are locally equal everywhere in the system. Finally, in the bottom right plots, the temperature ratio $\gamma \equiv T_1/T_2$ is shown as a function of the height z. There is a quite good agreement between the theoretical prediction $\gamma \approx 0.97$ and the simulation results, consistently with the fact that the two main hypotheses in which the theory is based, equality of the partial cooling rates and accuracy of the Gaussian local HCS approximation to compute them, have been seen to be verified in the present case. It is interesting to stress that, in spite of the large temperature and density gradients in some regions of the system, the value of the temperature ratio is practically uniform along it.

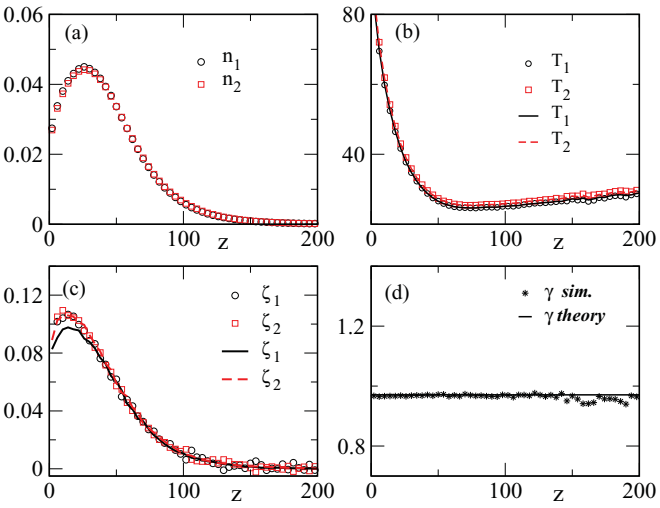

FIG. 3. (Color online) (a) Dimensionless density profiles $n_i\sigma^2$, (b) partial temperature profiles $T_i/m_1 g_0 \sigma$, (c) partial cooling rate profiles $\zeta_i\,(\sigma/g_0)^{1/2}$, and (d) temperature ratio profile $\gamma \equiv T_1/T_2$ for a mixture with $m_1 = m_2$, $\alpha_{11} = 0.92$, and $\alpha_{22} = 0.98$. The height z is measured in units of the diameter of the particles σ. The lines are the theoretical results obtained as discussed in the main text, while the symbols are from MD simulations.

To see the effect of the disparity of masses, consider now a system in which the mass of the less inelastic component (species 2) is larger than that of the more inelastic one (species 1), namely, $m_2 = 4m_1$. The results for the different profiles in this case are given in Fig. 4. A first consequence of the disparity of masses is that the density profiles of both components are quite different, with a larger concentration of the heavier particles close to the bottom of the system, as expected. Moreover, the heavier particles are more localized than the lighter ones, i.e., the density profile of the former is sharper. Also, from the density profiles, it follows that the concentration $c \equiv n_2/n_1$ depends strongly on height, exhibiting a maximum. With regard to the temperature profiles, it is seen that the difference between the partial temperatures is larger than in the case of equal masses. Moreover, the temperature of species 2 (less inelastic and heavier) shows a rapid increase with the height for $z \gtrsim 150\sigma$, where the density of this component has already decayed to rather small values $n_2(z = 150\sigma) \simeq 10^{-4}\sigma^{-2}$. This increase is not captured by the theory considered here, which, otherwise,

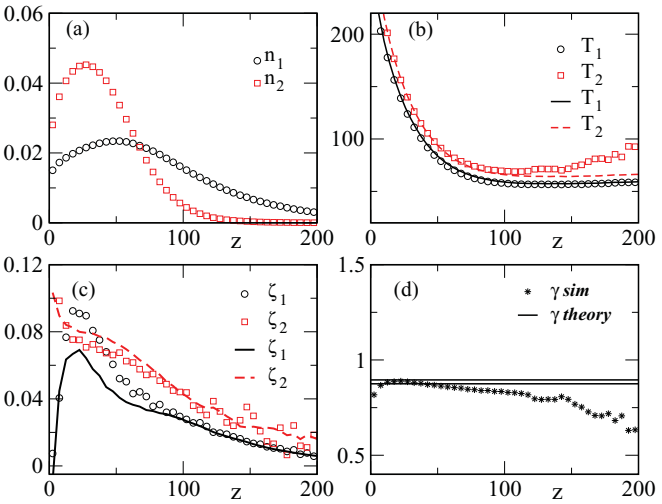

FIG. 4. (Color online) The same as in Fig. 3, but now $m_2 = 4m_1$. The two dashed lines in the plot of the temperature ratio γ have been obtained from Eq. (23) by using the the maximum and minimum values of the concentration n_2/n_1 in the system, as discussed in the main text.

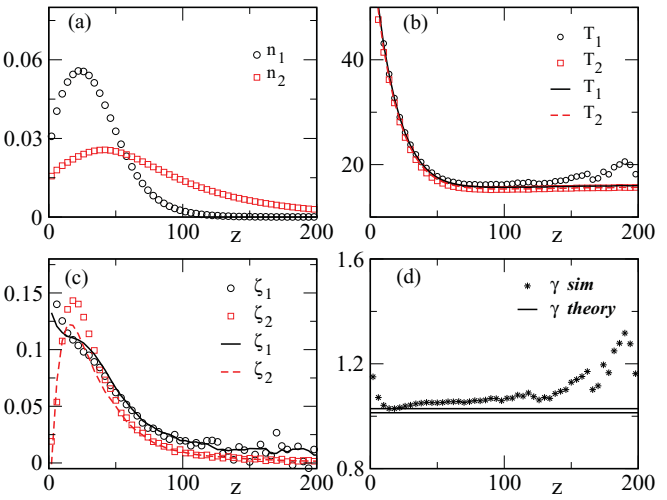

FIG. 5. (Color online) The same as in Fig. 3, but now $m_2 = m_1/4$. The two dashed lines in the plot of the temperature ratio γ have been obtained from Eq. (23) by using the the maximum and minimum values of the concentration n_2/n_1 in the system, as discussed in the main text.

turns out to be quite accurate for smaller heights, as well as for the complete temperature profile of the other component.

The profiles of the cooling rates in Fig. 4 are particularly illuminating. The MD results have a rather complicated structure that is well reproduced by the Gaussian local HCS approximation, away from a boundary layer in the vicinity of the density maximum for the lighter component. Moreover, although it is true that there is a neat discrepancy between the partial cooling rates of both components, they follow a similar trend and their difference remains relatively small. Note that, for $z \gtrsim 125\sigma$, the simulation data for the cooling rate of the component 2 are very noisy, due to its very low density in that region. Actually, the global density is also very small there, Knudsen effects are relevant, and hydrodynamics is not expected to apply. A similar comment applies near to the vibrating wall, say, $z \lesssim 5\sigma$. The width of the corresponding boundary layers can be estimated from the simulation data [34] and then restrict the comparison to the bulk region excluding the boundary layers at the bottom and top of the system. The values delimiting the bulk obtained in this way are close to those mentioned just above. Nevertheless, we have opted to present the raw data in the figures, without including any estimation of the boundary layers, since a detailed theory of the called kinetic layer and the transition regime [35] is not available for the system at hand.

The theoretical prediction for γ given by Eq. (23) has been computed for two extreme values of the concentration c, namely, $c = 2$ and 10^{-2}, which are roughly the maximum and minimum values of the concentration observed in the bulk of the system. The lowest and upper dashed lines in the bottom right plot of Fig. 4 correspond to the high and low concentration values, respectively. The agreement between theory and simulation results is not very good, as expected from the discrepancies observed for the local partial cooling rates of the two components. Nevertheless, it can be considered as satisfactory, especially if the boundary layers ($z \gtrsim 125\sigma$ and $z \lesssim 5\sigma$) are not taken into account for the reasons mentioned above.

Finally, the results for the case in which the more inelastic particles are the heavier ones are illustrated in Fig. 5, which corresponds to a system with $m_2 = m_1/4$. Since the conclusions following from the analysis are similar to those already discussed in the previous cases, they will be not reproduced again.

IV. SUMMARY AND DISCUSSION

The main result in this paper is twofold. First, it has been shown that, for a binary mixture of granular gases in an inhomogeneous state with strong temperature gradients, the Gaussian local HCS approximation provides a very accurate description of the partial (and total) cooling rates. In addition to the implication for the practical evaluation of the cooling rates, this property provides a justification for the form generally used for the hydrodynamic equations of granular gases to Navier-Stokes order. It indicates that the the first and second order in the gradient terms coming from the expansion of the exact cooling rates can be safely neglected. Of course, granular one-component systems are included as a limiting case. A third implication of this result is that it strongly supports the validity of a hydrodynamic description involving only the global local temperature and not the partial ones. The latter follow from the former and the partial density profiles.

The second main conclusion is that the equality of the local cooling rates of the components provides a quite useful relation to determine the ratio of the partial temperatures of the components, even though simulations show that deviations from this behavior occur if the masses of the components are different. The equality of the cooling rates is not an exact result following from kinetic theory, but a consequence of the mathematical procedure followed to obtain an approximated solution of the Enskog equations, namely, the expansion in

TABLE I. Comparison between the predictions from Eq. (23) and the MD results by Barrat and Trizac [6].

$\alpha_{11}, \alpha_{12}, \alpha_{22}$	m_1/m_2	T_2/T_1 (MD)	T_2/T_1 [Eq. (17)]
0.85, 0.85, 0.85	3	0.88	0.86
0.85, 0.85, 0.85	5	0.79	0.76
0.9, 0.8, 0.7	3	0.73	0.72
0.7, 0.8, 0.9	3	0.95	0.91

orthogonal Sonine polynomials. In this context, it is important to stress that the interest on the partial temperatures of the mixture goes beyond the formal result of the violation of equipartition. For instance, the expressions of the transport coefficients as derived formally in [10–12] involve the partial temperatures, which therefore must be computed in some way.

Most of the works studying the nonequipartition of energy in granular mixtures consider the steady state reached by a system with one (or two) vibrating boundaries. Barrat and Trizac [6] have reported MD results for the temperature ratio in a vibrated granular mixture of inelastic hard disks. The diameters of the particles are always taken the same, $\sigma_1 = \sigma_2$, as in the work being reported here. The global area fraction is $\nu = 0.04$. A comparison between their results and the predictions of Eq. (23) is given in Table I. Since the number of particles of both species is the same in the simulations, we have taken $n_1/n_2 = 1$. The agreement is quite good.

The temperature ratio in two-dimensional vibrated granular mixtures has been measured experimentally by Feitosa and Menon [8]. They use spheres of the same size and different materials. Their main qualitative conclusions are as follows.

(1) The temperature ratio does not depend on the vibration velocity of the walls. This is consistent with the results derived here and, in particular, with the independence of γ from the hydrodynamic gradients, which are determined by the intensity of the vibration.

(2) The temperature ratio strongly depends on the mass ratio of the components, being an increasing function of it. This feature also agrees with the theoretical prediction given by Eq. (23), as illustrated in Fig. 1.

(3) The ratio is insensitive to the area fraction of the mixture and of each component. The former follows from the fact that, when all the diameters are equal, g_{ij}, as given by Eq. (18), is the same for all i, j, and therefore Eq. (17) becomes independent of ν. The weak dependence on composition is illustrated in Fig. 1.

For a mixture of glass and aluminium with mass ratio $m_1/m_2 \simeq 0.92$, they measure a value of γ very close to unity, while for mixtures of steel and glass ($m_1/m_2 \simeq 0.29$) and brass and glass ($m_1/m_2 \simeq 0.33$), they find $\gamma \simeq 0.66$ and 0.69, respectively. To evaluate the predictions from Eq. (17), the restitution coefficients are needed. The authors only report the values of some effective inelasticity coefficients from which it is not clear how to deduce the coefficients α_{ij}. As a rough estimation, the values of the restitution coefficients employed in Fig. 1 can be used. Then, discrepancies of the order of 25% are obtained. This is not unsatisfactory since, in addition to all the approximations made, it must be taken into account that, in the experiments, the beads can rotate in three dimensions and rotational friction is neglected in the present theory.

Another series of experiments measuring γ has been carried out by Wildman and Parker [9]. They use two sizes of glass spheres ($d = 3$) with $\sigma_1/\sigma_2 = 5/4$, and estimate $\alpha_{11} = \alpha_{22} = 0.91$. In the region where the temperature ratio is measured, it is $\nu \sim 10^{-3}$, so that, with very good accuracy, $g_{ij} \approx 1$. By changing the number fraction of the two species, they identify a weak dependence of γ on n_1/n_2. Taking for n_1/n_2 the value of the ratio between the total number of particles of each species, we get $\gamma = 1.029$, 1.027, and 1.026 for the three cases considered in [9], while the reported experimental results are 1.41, 1.27, and 1.25, respectively. The qualitative behavior is the same, and for the reasons discussed above, the quantitative agreement can not be considered as bad.

In summary, Eq. (23) is consistent with both simulation and experimental results. This seems to confirm its validity and also the accuracy of a hydrodynamic description involving only the temperature of the mixture.

ACKNOWLEDGMENT

This research was supported by the Ministerio de Educación y Ciencia (Spain) through Grant No. FIS2011-24460 (partially financed by FEDER funds).

[1] J. T. Jenkins and F. Mancini, J. Appl. Mech. **54**, 27 (1987).
[2] V. Garzó and J. Dufty, Phys. Rev. E **60**, 5706 (1999).
[3] S. R. Dahl, C. M. Hrenya, V. Garzó, and J. W. Dufty, Phys. Rev. E **66**, 041301 (2002).
[4] A. Barrat and A. Trizac, Granular Matter **4**, 57 (2002).
[5] J. E. Galvin, S. R. Dhal, and C. M. Hrenya, J. Fluid Mech. **528**, 207 (2005).
[6] A. Barrat and E. Trizac, Phys. Rev. E **66**, 051303 (2002).
[7] R. Brito, H. Enriquez, S. Godoy, and R. Soto, Phys. Rev. E **77**, 061301 (2008).
[8] K. Feitosa and N. Menon, Phys. Rev. Lett. **88**, 198301 (2002).
[9] R. D. Wildman and D. J. Parker, Phys. Rev. Lett. **88**, 064301 (2002).
[10] V. Garzó and J. W. Dufty, Phys. Fluids **14**, 1476 (2002).
[11] V. Garzó and J. M. Montanero, J. Stat. Phys. **129**, 27 (2007).
[12] V. Garzó, J. W. Dufty, and C. M. Hrenya, Phys. Rev. E **76**, 031303 (2007).
[13] An exception is J. J. Brey, J. W. Dufty, C. S. Kim, and A. Santos, Phys. Rev. E **58**, 4638 (1998), where some contributions to the cooling rate proportional to the Laplacian of the hydrodynamic fields are investigated.
[14] J. J. Brey, J. W. Dufty, and A. Santos, Physica **87**, 1051 (1997).
[15] H. Idir and H. Arastoopour, AIChE J. **51**, 1620 (2005).
[16] J. W. Dufty and J. J. Brey, Math. Model. Nat. Phenom. **6**, 19 (2011).
[17] J. M. Montanero and V. Garzó, Granular Matter **4**, 17 (2002).

[18] J. J. Brey and M. J. Ruiz-Montero, Phys. Rev. E **80**, 041306 (2009).
[19] J. H. Ferziger and H. G. Karper, *Mathematetical Theory of Transport Processes in Gases* (North-Holland, Amsterdam, 1972).
[20] J. W. Dufty, J. J. Brey, and J. Lutsko, Phys. Rev. E **65**, 051303 (2002).
[21] J. J. Brey, M. J. Ruiz-Montero, and F. Moreno, Phys. Rev. Lett. **95**, 098001 (2005).
[22] J. J. Brey, M. J. Ruiz-Montero, and F. Moreno, Phys. Rev. E **73**, 031301 (2006).
[23] J. A. McLennan, *Introduction to Nonequilibrium Statistical Mechanics* (Prentice Hall, New Jersey, 1989).
[24] P. Résibois and M. de Leener, *Classical Kinetic Theory of Fluids* (Wiley-Interscience, New York, 1977).
[25] E. W. Grundke and D. Henderson, Mol. Phys. **24**, 269 (1972).
[26] L. Verlet and D. Levesque, Mol. Phys. **46**, 969 (1982).
[27] S. McNamara and S. Luding, Phys. Rev. E **58**, 813 (1998).
[28] J. J. Brey, M. J. Ruiz-Montero, and F. Moreno, Phys. Rev. E **63**, 061305 (2001).
[29] P. Sunthar and V. Kumaran, Phys. Rev. E **64**, 041303 (2001).
[30] C. M. Hrenya, J. E. Galvin, and R. D. Wildman, J. Fluid Mech. **08**, 429 (2008).
[31] J. J. Brey and M. J. Ruiz-Montero, Europhys. Lett. **66**, 805 (2004).
[32] A. Goldshtein and M. Shapiro, J. Fluid Mech. **282**, 75 (1995).
[33] T. P. C. van Noije and M. Ernst, Granular Matter **1**, 57 (1998).
[34] J. E. Galvin, C. M. Hrenya, and R. D. Wildman, J. Fluid Mech. **585**, 73 (2007).
[35] C. Cercignani, *Theory and Application of the Boltzmann Equation* (Scottish Academic Press, London, 1975).